Topological Quantum Phases of ^{4}He Confined to Nanoporous Materials

Lode Pollet
Department of Physics, Arnold Sommerfeld Center for Theoretical Physics and Center for NanoScience, University of Munich, Theresienstrasse 37, 80333 Munich, Germany

Anatoly B. Kuklov
Department of Engineering Science and Physics, CUNY, Staten Island, New York 10314, USA
(Received 1 March 2014; revised manuscript received 21 April 2014; published 21 July 2014)

The ground state of ^{4}He confined in a system with the topology of cylinder can display properties of solid, superfluid, and liquid crystal. This phase, which we call a compactified supersolid (CSS), originates from wrapping the basal planes of the bulk hcp solid into concentric cylindrical shells, with several central shells exhibiting superfluidity along the axial direction. Its main feature is the presence of a topological defect which can be viewed as a disclination with Frank index $n = 1$ observed in liquid crystals, and which, in addition, has a superfluid core. The CSS as well as its transition to an insulating compactified solid with a very wide hysteresis loop are found by *ab initio* Monte Carlo simulations. A simple analytical model captures qualitatively correctly the main property of the CSS—a gradual decrease of the superfluid response with increasing pressure.

DOI: 10.1103/PhysRevLett.113.045301 PACS numbers: 67.80.bd, 67.80.bf

The emergence of unexpected phenomena in simple systems is one of the central themes in physics. A historic example is ^{4}He consisting of structureless bosons which, in addition to the classical phases, can exhibit macroscopic quantum behavior—superfluidity. Whether the crystalline and superfluid orders can occur simultaneously and form a supersolid is a question that still captivates the community 45 years after it was proposed [1]. While no supersolid has been seen in ideal hcp samples, some grain boundaries and dislocations have been found to support superfluidity in *ab initio* simulations [2,3] and, possibly, in the experiment [4]. A metastable phase, superglass, has also been observed in the simulations [5].

In apparently different fields, the emergence of quantum liquid crystals [6] has been proposed in such contexts [7] as the quantum Hall effect, bilayer $Sr_3Ru_3O_7$, the cuprates, and highly magnetic dipolar degenerate fermionic cold atoms [8] such as Cr [9], Er [10], and Dy [11], and for population imbalanced Fermi gases [12]. The role of curved substrate in inducing novel 2D phases was discussed in Ref. [13].

In this Letter, we reveal a phase induced by geometrical confinement, the compactified supersolid (CSS). This phase features topological properties of a liquid crystal as well as the quantum phenomenon of superfluidity. Our *ab initio* simulations show that a CSS must occur in ^{4}He confined to materials with a cylindrical geometry with a mesoscopic diameter not larger than 30 nm (see below), that is, in Vycor glass or in artificially made nanopores. Because of its topological nature, the CSS is robust against smooth deformations of the pores or disorder, implying that simulations inside an ideal cylinder are sufficient for elucidating its main features. There are also, as we will see, experimental signatures consistent with its existence. The description of CSS as well as of the compactified solid (CS) naturally invokes variables, objects, and terminology typical for liquid crystals. These are the smectic-*A*-type layers with the local hcp axis playing the role of the nematic-type director characterized by the splay and forming a disclination with Frank index $n = 1$ (see, e.g., Ref. [14]).

We start with discussing the similarity between the roton-induced spatial density modulation in superfluid ^{4}He close to a hard wall [15] and layers in classical smectic-*A* liquid crystals. Such a modulation as well as the liquid crystal layers both exhibit zero shear response in the tangential directions. If the hard wall has a cylindrical shape, the crests and troughs of the modulation acquire the cylindrical shape and form a structure containing Frank's disclination observed in liquid crystals [see Fig. 2(a) in Ref. [16]]. At high pressure, the modulation transforms into shells of the CS hereby freezing the disclination with its long-range splay. This splay may partially melt a few shells in the vicinity of the disclination line resulting in the CSS. This mechanism is similar to the strain-induced superfluid core of some dislocations in hcp ^{4}He [17]. There is, though, a significant difference between the two: In contrast to dislocations, the disclination is a part of the ground state of the CSS and CS. In our simulations we have observed both phases as well as the transformation between them characterized by a very wide hysteresis which implies that rather long-lived metastable superfluidity can exist at pressures much higher than in macroscopic 3D samples of solid ^{4}He.

The compactified structural order of ^{4}He has previously been observed numerically. A variational study [18] has

found that ^{4}He forms shells concentric with the pore wall. These shells are hexagonal layers rolled into cylinders which are claimed to be always superfluid. *Ab initio* Monte Carlo (MC) simulations [19] at saturated vapor pressure have equally found the shell structure, but with no intrashell structural order. While a pore with a diameter $R_0 = 2.9$ Å is insulating, a pore with $R_0 = 14$ Å demonstrates weak superfluidity.

Model description.—Here we introduce the relevant coarse grained variables and sketch the description of the main features of CSS and CS. The key variable is the envelope $\vec{C}(\vec{r})$ of the gradient of the density modulation at the roton wave vector k_r. In the liquid phase ^{4}He is characterized by a structure factor with the peak at k_r. In real space such a peak implies that the boundary induces spatially decaying density oscillations $\rho'(\vec{r}) \sim \exp(-i\vec{k}\,\vec{r}) + \text{c.c.}$ with $|\vec{k}| \approx k_r$ and the exponentially decaying part (k has an imaginary part) determined by the roton gap [15]. In a cylindrical geometry the modulation picks up the cylindrical symmetry $\rho'(r) \sim \exp(ik_r r) + \text{c.c.}$, where r is the radial coordinate. Accordingly, $\vec{C}(\vec{r}) \sim k_r \vec{r}/r$ winds around the cylinder axis in the same manner as the director field does in a liquid smectic-A crystal containing the disclination with Frank index $n = 1$. At high pressure, the modulations become crystalline shells which, in addition to the director field $\vec{C}$ setting the local orientation of the hcp axis, must be also described by the intrashell (quasi-) hexagonal order.

Similarly to liquid crystals, the contributions of $\vec{C}$ to the energy can be characterized by splay, twist, and bend as well as by shell deformations. Given the simplest geometry, we ignore twist and bend and consider only the splay energy

$$E_s \sim \int d^2 r dz (\vec{\nabla}\,\vec{C})^2 \sim \ln(R_0/R) L_z. \tag{1}$$

Here, z is the coordinate along the cylindrical axis, L_z stands for the total length of the cylinder, R_0 denotes the cylinder radius, and $R < R_0$ is the radius of the disclination core inside which the splay singularity $\vec{\nabla}\,\vec{C} \sim 1/r$ has been cured by melting the inner shells into a superfluid (characterized by a complex field ψ as another order parameter). Thus, while being of the order of the interparticle distance in the CS phase with $\psi = 0$, R can be mesoscopically large in the CSS phase so that there is $\psi \neq 0$ inside the core. In the simulations we associate the CSS to CS transition with the vanishing of superfluidity.

Melting of the core above the melting pressure $P_m \sim 25$ bar costs energy $E_c \approx (\mu_l - \mu_s) R^2 L_z$, where $\mu_l > \mu_s$ stand for the chemical potentials of liquid and solid, respectively. Thus, the equilibrium solution for the core radius can be found by minimizing the total CSS energy $E_s + E_c$ with respect to R. This gives $R \propto 1/\sqrt{\mu_l - \mu_s}$ where we ignore the surface tension and assume the limit $R \ll R_0$. As the external pressure P increases above P_m, the core radius decreases and so does the superfluid response $\rho_s \propto R^2$:

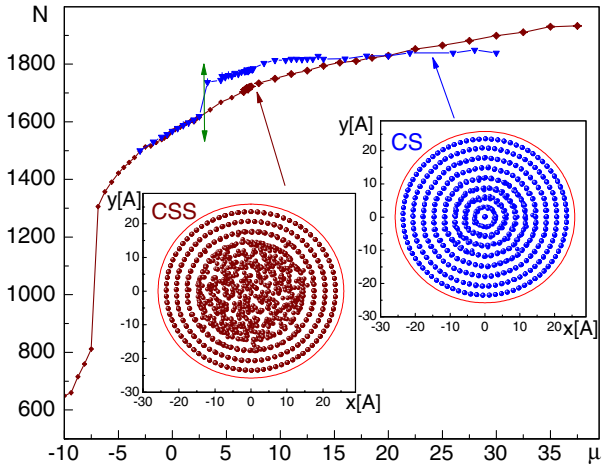

FIG. 1 (color online). The number of particles N vs chemical potential μ for two phases CSS and CS. The double-sided arrow indicates the ending of the hysteresis at $\mu \approx 3.2$ K. Insets: columnar view along the cylindrical axis of a typical atomic configuration of CSS (left) and CS (right) both at $\mu = 7.1$ K. The solid (red) circle outlines the pore boundary at $R = R_0$. The quasidisordered region in the CSS is the superfluid core.

$$\rho_s \propto \frac{1}{P - P_m}, \tag{2}$$

where we used $\mu_l - \mu_s \sim P - P_m$. Equation (2) is qualitatively consistent with the simulations (see Fig. 2) and with the experimental observations [20] of ^{4}He in Vycor.

Ab initio simulations—We have conducted *ab initio* MC simulations (by the worm algorithm [21,22]) of a grand-canonical ensemble at various values of chemical potential μ so that there are $N \sim 600$–2000 ^{4}He atoms confined inside a cylindrical volume with periodic boundary conditions along the z direction ($L_z = 30$ Å) at temperature $T = 0.2$ K. In the Hamiltonian,

$$H = -\frac{\hbar^2}{2m} \sum_{i=1}^{N} \vec{\nabla}_i^2 + \sum_{i<j} V_{\text{Aziz}}(r_{ij}) + \sum_i V_{\text{sub}}(\vec{r}_i), \tag{3}$$

$(\hbar^2/2m)\vec{\nabla}_i^2$ is the kinetic energy operator of ith ^{4}He atom located at $\vec{r}_i$; $V_{\text{Aziz}}(r_{ij})$ is the standard central Aziz-potential [23], with $r_{ij} \equiv |\vec{r}_i - \vec{r}_j|$. The potential $V_{\text{sub}} = D/2(b^9/\xi^9 - 3(b^3/\xi^3))$, with $b = 2.0$ Å and $D = 80$ K, acts between the pore wall and ^{4}He atoms. It is the so called 3–9 potential [19], where in the cylindrical geometry $\xi = R_0 - r > 0$, with $R_0 = 25.8$ Å. The precise shape of $V_{\text{sub}}(\boldsymbol{r}_i)$ does not change anything qualitatively (cf. Ref. [24]) as long as its depth $D = 80$ K is much bigger than that ($\approx$11 K) of $V_{\text{Aziz}}(r_{ij})$.

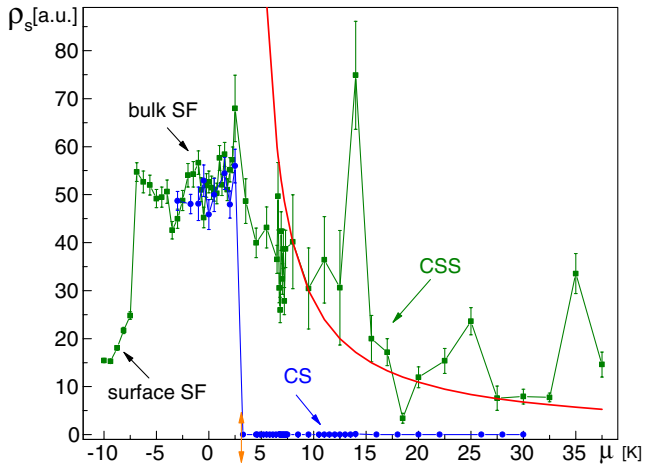

FIG. 2 (color online). Superfluid stiffness ρ_s vs μ of ^{4}He in the nanopore. The solid red line is the fit by Eq. (2). The double-sided arrow indicates the closing of the hysteresis loop.

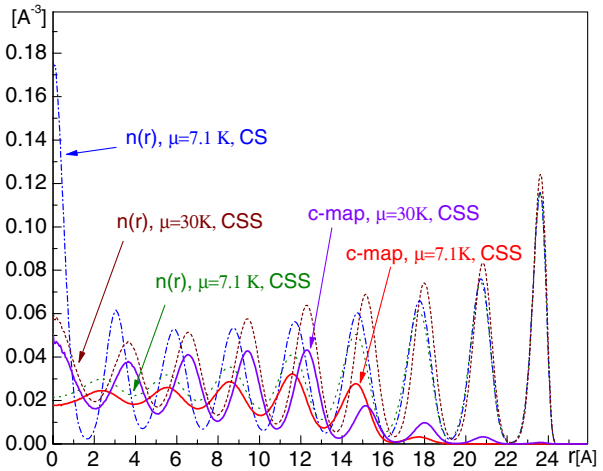

FIG. 3 (color online). Atomic, $n(r)$, and condensate, c-map, densities along the radial direction in the samples corresponding to $\mu = 7.1$ and 30 K.

A typical atomic configuration of the CSS, shown in the left inset in Fig. 1, features well-defined outer shells (3 of them at $\mu = 7.1$ K), each with slightly distorted hexagonal order (shown in Figs. 4 and 5 in the Supplemental Material [25]), as well as the superfluid core which is visibly disordered (within the radius $R \sim 12$–15 Å). Most of the superfluid response seen in Fig. 2 comes from this core. Despite being apparently fully disordered, there are distinct radial density $n(r)$ as well as superfluid density (represented by the so-called condensate map or c map, see in Ref. [5]) modulations in the core seen in Fig. 3. Increasing μ in the CSS phase leads to the compression of the superfluid core and to the gradual suppression of the superfluid stiffness ρ_s. The core compression can be recognized in Fig. 3: The concentration of the c map in the center is higher in the $\mu = 30$ K sample than in the $\mu = 7.1$ K one. The red line in Fig. 2 is the fit by Eq. (2) of the numerically found ρ_s, where we have used $(P-P_m) \propto (\mu-\mu_m)$, with μ_m corresponding to the melting of macroscopic hcp samples (with no disclination). In order to find μ_m, we ran simulations in the slab geometry, that is, with a flat smooth wall and periodic boundary conditions along the wall producing the same 3–9 potential $V_{\rm sub}$. We found the solid spinodal at $\mu = \mu_{\rm sp} \approx 3.0$ K, and the liquid spinodal at about 7 K. In the experiment [26] it has been determined that the solid spinodal pressure is below P_m by about 10–15%. Thus, we estimate $\mu_m \approx 1.15\mu_{\rm sp} \approx 3.5$ K. On top of the overall suppression of ρ_s vs μ in Fig. 2 consistent with Eq. (2) there are additional peaks and dips in ρ_s vs μ (see Fig. 2), which may be related to structural fluctuations caused by the proximity to the CS phase.

The emergence of various phases in the pore is reflected in the dependence of the particle number N vs μ in Fig. 1. At $\mu < -50$ K, the outermost shell becomes populated and forms a superfluid. It solidifies into a hexagonal (insulating) shell at $\mu \approx -30$ K. [This stage is not reflected in Fig. 1.] The second shell forms in the range $-12 < \mu < -7$ K. It is a low density surface superfluid (SF) which exhibits no visible structural order (see Fig. 1 of the Supplemental Material [25]). Accordingly, the curves in Figs. 1 and 2 show linear dependencies on μ in this range. During this stage the pore bulk remains empty. At $\mu \approx -7$ K ^{4}He undergoes a dimensional crossover marked by the jumps in N (Fig. 1) and in the superfluid stiffness ρ_s (Fig. 2): at $\mu > -7$ K the whole pore becomes filled by ^{4}He forming a low density superfluid. In this phase, while only two outer shells are clearly defined and possess hexagonal order, the weak radial density modulations induced by the roton [15] can also be detected in the pore bulk (see Fig. 2 in the Supplemental Material [25]).

The CS begins as a metastable phase at $\mu \approx 3.2$ K as shown in Fig. 1. The shells (we observed eight of them) of the CS are well defined and exhibit hexagonal order consistent with the whole hcp crystal being compactified (see the Supplemental Material [25] for details). There is also a central (insulating) core hosting ^{4}He atoms along a very narrow straight line coinciding with the cylinder axis. The CS phase is characterized by zero superfluid response $\rho_s = 0$ as seen in Fig. 2. A weak dependence of N vs μ of the CS shown in Fig. 1 indicates that doping is still possible in this insulating state. However, the extra particles (or vacancies) do not form a superfluid. Instead, they phase separate, very similarly to the case of macroscopic samples studied in Ref. [27]. Lowering μ below $\mu \approx 3.2$ K results in a jumplike melting of the CS into the bulk SF (which gradually transforms into the CSS as μ increases). This indicates closing of the hysteresis at its low end as marked by the double sided arrows in the curves N vs μ (Fig. 1) and in ρ_s vs μ (Fig. 2).

While the CS is metastable at 3.2 K $< \mu <$ 7–10 K, the CSS is stable in this region and becomes metastable above $\mu \approx 7$–10 K. Because of the very wide hysteresis a more

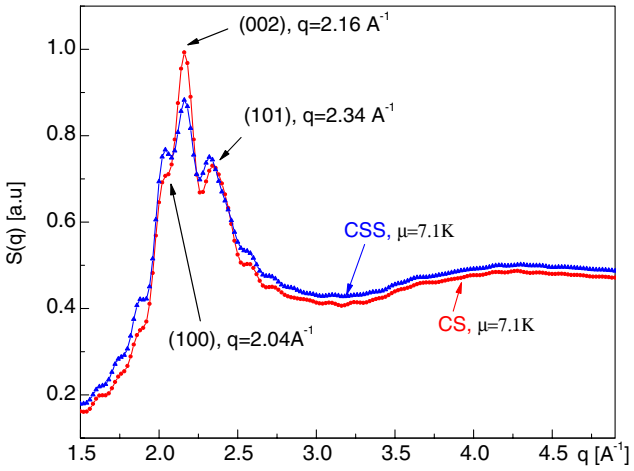

FIG. 4 (color online). Structure factors of CSS and CS averaged over orientations. The major peaks are labeled according to the standard hcp classification.

accurate finding of the transition point turned out to be very challenging. As Fig. 1 indicates, the upper end of the hysteresis, where the metastable CSS transforms into the stable CS, could not be determined: the CSS persisted at μ as high as 38 K, in sharp contrast to the results in the slab geometry with the hysteresis loop being only 4 K wide (see above).

Discussion.—One of the longstanding open questions is the nature of solid ^{4}He in a Vycor. Superfluidity there persists at a pressure P as high as 10–20 bar above the melting pressure. Several models have been proposed to explain this effect [20,28–30], including the conjecture that ^{4}He remains liquid close to the Vycor wall with the solid forming away from the wall [20]. MC simulations of about 200 ^{4}He atoms [31] with the artificially fixed hcp solid at some small distance from the wall support this picture. As our simulations of bigger samples in a realistic geometry show, there is no liquid layer adjacent to the wall, and, instead, there is a liquid core at the pore center. We also note that our observations are in contrast to the variational results [18] predicting that the solid in a nanopore is always a supersolid.

The wetting models [20,28,29], where ^{4}He at the wall remains liquid until pressure overcomes the surface tension nucleation barrier, encounter troubles explaining the gradual decrease of the superfluid response with pressure [20] because the nucleation mechanism implies an abrupt solidification. In contrast, the CSS is characterized by a gradual decrease of its superfluid response with pressure. The experimental observation of the overall decrease of entropy of the liquid part of ^{4}He in Vycor with increasing pressure, seen in Fig. 1(c) of Ref. [32], is also consistent with the shrinking of the superfluid core with pressure observed in our simulations.

Our analysis and simulations of the topological phases of ^{4}He in nanopores are directly relevant to pores with radii below a threshold, $R_{\max} \sim 300$ Å (as estimated in the Supplemental Material [25]), well above typical radii in Vycor or Gelsil glass. We consider it a lower bound because the CS or CSS may exist as metastable phases in much larger pores due to the geometrical (macroscopic) energy barrier between the compactified and standard hcp solids. This implies that the CSS can be grown and studied in a more controlled way in artificially created pores.

In the recent experiment [33], ^{4}He in Vycor was found to be in the bcc phase at $P < 98$ bar and $T \approx 0.5$–0.7 K, whereas the transformation to the hcp solid takes place at higher pressure. The structure factor for CS and CSS (averaged over all orientations) found in our simulations and shown in Fig. 4 is strikingly similar to the one found in Ref. [33] at high pressure. It features three main peaks in the momentum region $\sim$2.0–2.2 Å^{-1}: one strong and two satellite peaks reminiscent of the three main Bragg peaks of hcp solid. The higher order peaks are washed out by quantum fluctuations and are "hidden" under the wide shoulder at high momenta. In future work it would be important to repeat the experiment [33] at lower temperatures, as well as to perform the MC simulations at temperatures higher than $T = 0.2$ K. One possibility is that there is a nontrivial transition line in the P-T plane where the compactified hcp solid becomes a compactified bcc solid.

Finally, we suggest (and leave the analysis for future work) that the CSS disclinations ending at the interface of Vycor and the bulk solid ^{4}He may attract (and also create) the bulk dislocations with superfluid cores [3], so that the superflow through the bulk becomes possible as observed in Ref. [4].

Conclusion.—When ^{4}He is subjected to geometrical confinement with cylindrical topology, it can be found in the compactified solid and compactified supersolid phases. Both are characterized by the shelled structure reminiscent of smectic-A liquid crystal containing Frank's disclination. While the CS is insulating, the CSS exhibits superfluid response within the melted core of the disclination. Such a core can persist in a metastable state at pressures significantly exceeding the spinodal for the overpressured superfluid in macroscopic samples of ^{4}He. This finding offers a compelling explanation for the physics of ^{4}He confined to restricted geometries at high pressure where the local C_6 axis, playing the role of the nematic director, cannot be uniquely defined everywhere. Thus, in the multiple-connected geometry of nanoporous materials confining ^{4}He the superfluid response at high pressure should be controlled by a network of the disclinations.

We wish to thank M. Boninsegni, A. Del Maestro, R. Hallock, N. Mulders, and Boris Svistunov for fruitful discussions. This work was supported by FP7/Marie-Curie Grant No. 321918 ("FDIAGMC"), FP7/ERC Starting

Grant No. 306897; by the NSF Grant No. PHY1314469, and by the Grant from CUNY HPCC under NSF Grants No. CNS-0855217, No. CNS-0958379, and No. ACI-1126113.

[1] A. F. Andreev and I. M. Lifshitz, Sov. Phys. JETP **29**, 1107 (1969); D. J. Thouless, Ann. Phys. (N.Y.) **52**, 403 (1969); G. V. Chester, Phys. Rev. A **2**, 256 (1970); A. J. Leggett, Phys. Rev. Lett. **25**, 1543 (1970).
[2] L. Pollet, M. Boninsegni, A. B. Kuklov, N. V. Prokof'ev, B. V. Svistunov, and M. Troyer, Phys. Rev. Lett. **98**, 135301 (2007).
[3] M. Boninsegni, A. B. Kuklov, L. Pollet, N. V. Prokof'ev, B. V. Svistunov, and M. Troyer, Phys. Rev. Lett. **99**, 035301 (2007); S. G. Söyler, A. B. Kuklov, L. Pollet, N. V. Prokof'ev, and B. V. Svistunov, Phys. Rev. Lett. **103**, 175301 (2009).
[4] M. W. Ray and R. B. Hallock, Phys. Rev. Lett. **100**, 235301 (2008); Ye. Vekhov and R. B. Hallock, Phys. Rev. Lett. **109**, 045303 (2012).
[5] M. Boninsegni, N. Prokof'ev, and B. V. Svistunov, Phys. Rev. Lett. **96**, 105301 (2006).
[6] S. A. Kivelson, E. Fradkin, and V. J. Emery, Nature (London) **393**, 550 (1998).
[7] E. Fradkin, S. Kivelson, M. J. Lawler, J. P. Eisenstein, and A. P. Mackenzie, Annu. Rev. Condens. Matter Phys. **1**, 153 (2010).
[8] B. M. Fregoso, K. Sun, E. Fradkin, and B. L. Lev, New J. Phys. **11**, 103003 (2009).
[9] A. Griesmaier, J. Werner, S. Hensler, J. Stuhler, and T. Pfau, Phys. Rev. Lett. **94**, 160401 (2005).
[10] J. J. McClelland and J. L. Hanssen, Phys. Rev. Lett. **96**, 143005 (2006).
[11] M. Lu, N. Q. Burdick, and B. L. Lev, Phys. Rev. Lett. **108**, 215301 (2012).
[12] L. Radzihovsky and A. Vishwanath, Phys. Rev. Lett. **103**, 010404 (2009).
[13] M. J. Bowick, D. R. Nelson, and A. Travesset, Phys. Rev. B **62**, 8738 (2000).
[14] L. D. Landau and E. M. Lifshitz, *Course of Theoretical Physics; Theory of Elasticity*, 3rd ed. (Elsevier Ltd., Oxford, UK, 1986), Vol. 7.
[15] F. Dalfovo, A. Lastri, L. Pricaupenko, S. Stringari, and J. Treiner, Phys. Rev. B **52**, 1193 (1995).
[16] R. Bidaux, N. Boccara, G. Sarma, L. de Seze, P. G. de Gennes, and O. Parodi, J. Phys. (France) **34**, 661 (1973).
[17] L. Pollet, M. Boninsegni, A. B. Kuklov, N. V. Prokof'ev, B. V. Svistunov, and M. Troyer, Phys. Rev. Lett. **101**, 097202 (2008); **101**, 269901(E) (2008).
[18] M. Rossi, D. E. Galli, and L. Reatto, Phys. Rev. B **72**, 064516 (2005).
[19] A. Del Maestro, M. Boninsegni, and I. Affleck, Phys. Rev. Lett. **106**, 105303 (2011).
[20] C. Lie-zhao, D. F. Brewer, C. Girit, E. N. Smith, and J. D. Reppy, Phys. Rev. B **33**, 106 (1986).
[21] M. Boninsegni, N. Prokof'ev, and B. Svistunov, Phys. Rev. Lett. **96**, 070601 (2006).
[22] M. Boninsegni, N. V. Prokof'ev, and B. V. Svistunov, Phys. Rev. E **74**, 036701 (2006).
[23] R. A. Aziz, V. P. S. Nain, S. Carley, W. L. Taylor and G. T. McConville, J. Chem. Phys. **70**, 4330 (1979).
[24] M. Boninsegni, J. Low Temp. Phys. **159**, 441 (2010).
[25] See Supplemental Material at http://link.aps.org/supplemental/10.1103/PhysRevLett.113.045301 for additional illustration and information of the surface phase as well as the CS and CSS phase.
[26] F. Souris, J. Grucker, J. Dupont-Roc, and Ph. Jacquier, Europhys. Lett. **95**, 66001 (2011).
[27] M. Boninsegni, A. B. Kuklov, L. Pollet, N. V. Prokof'ev, B. V. Svistunov, and M. Troyer, Phys. Rev. Lett. **97**, 080401 (2006).
[28] J. G. Dash, Phys. Rev. B **25**, 508 (1982).
[29] J. R. Beamish, A. Hikata, L. Tell, and C. Elbaum, Phys. Rev. Lett. **50**, 425 (1983).
[30] D. N. Bittner and E. D. Adams, J. Low Temp. Phys. **97**, 519 (1994).
[31] S. A. Khairallah and D. M. Ceperley, Phys. Rev. Lett. **95**, 185301 (2005).
[32] K. Yamamoto, Y. Shibayama, and K. Shirahama, Phys. Rev. Lett. **100**, 195301 (2008).
[33] S. Bera, J. Maloney, L. B. Lurio, N. Mulders, Z. G. Cheng, M. H. W. Chan, C. A. Burns, and Z. Zhang, Phys. Rev. B **88**, 054512 (2013).